Joe Tien[1]
Department of Biomedical Engineering,
Boston University,
Boston, MA 02215;
Division of Materials Science and Engineering,
Boston University,
Boston, MA 02215
e-mail: jtien@bu.edu

Le Li
Department of Mechanical Engineering,
Boston University,
Boston, MA 02215;
Photonics Center,
Boston University,
Boston, MA 02215

Ozgur Ozsun
Department of Mechanical Engineering,
Boston University,
Boston, MA 02215;
Photonics Center,
Boston University,
Boston, MA 02215

Kamil L. Ekinci[1]
Department of Mechanical Engineering,
Boston University,
Boston, MA 02215;
Division of Materials Science and Engineering,
Boston University,
Boston, MA 02215;
Photonics Center,
Boston University,
Boston, MA 02215
e-mail: ekinci@bu.edu

Dynamics of Interstitial Fluid Pressure in Extracellular Matrix Hydrogels in Microfluidic Devices

In order to understand how interstitial fluid pressure and flow affect cell behavior, many studies use microfluidic approaches to apply externally controlled pressures to the boundary of a cell-containing gel. It is generally assumed that the resulting interstitial pressure distribution quickly reaches a steady-state, but this assumption has not been rigorously tested. Here, we demonstrate experimentally and computationally that the interstitial fluid pressure within an extracellular matrix gel in a microfluidic device can, in some cases, react with a long time delay to external loading. Remarkably, the source of this delay is the slight (∼100 nm in the cases examined here) distension of the walls of the device under pressure. Finite-element models show that the dynamics of interstitial pressure can be described as an instantaneous jump, followed by axial and transverse diffusion, until the steady pressure distribution is reached. The dynamics follow scaling laws that enable estimation of a gel's poroelastic constants from time-resolved measurements of interstitial fluid pressure. [DOI: 10.1115/1.4031020]

Keywords: poroelasticity, hydrogel, microfluidics, soft materials, interstitial pressure

Introduction

The interstitial fluid that suffuses a living tissue transmits important signals that affect the behavior of cells within that tissue [1]. These signals include the normal and shear stresses that are exerted by interstitial fluid pressure and flow, respectively, and the polarized solute concentration profiles that result from interstitial convection [2,3]. Ultimately, the common origin of these signals is the spatial and temporal distribution of interstitial fluid pressure [4].

As a porous and elastic (poroelastic) solid that is saturated with fluid, a biological tissue is dragged and thus deformed by interstitial flow [5,6]. Conversely, changes in tissue porosity will alter the interstitial fluid pressure and resulting flow field [7]. This coupling between the interstitial fluid and solid constituents is well-appreciated for some tissues (e.g., cartilage) [8,9], but less so for the highly porous hydrogels and engineered tissues often used in culture. Many recent studies have subjected cell-laden hydrogels in microfluidic devices to changes in interstitial pressure gradients [10,11], and these studies tacitly assumed that the local interstitial pressure and flow respond instantaneously, or nearly so, to changes in the external pressure conditions.

In this study, we examine how interstitial fluid pressure changes with external loading in a microfluidic device that contains a biological gel. We used a combination of experimental and numerical approaches to discover that pressure changes within extracellular matrix gels (type I collagen, fibrin, and Matrigel) can be remarkably slow, and that the timescale for these changes depends not only on the poromechanical properties of the gel but also on the elastic properties of the material that the gel is in contact with. When a poroelastic gel is subjected to a change in external stress, it responds instantaneously (the undrained deformation) and then gradually reaches a steady-state (the drained deformation) [7]. The transition from undrained to drained behavior can be described by the diffusion of interstitial pressure and strain, with a diffusion constant that depends solely on the hydraulic permeability and elastic modulus of the gel. We now show that the presence of a deformable boundary (such as the wall of a microfluidic device) in contact with the porous gel introduces a second diffusion constant, one that depends on the elastic modulus of the surroundings. The deformation of the gel follows a universal scaling law, which allows determination of the gel's poromechanical properties from noninvasive, time-lapse measurements of interstitial fluid pressure.

Materials and Methods

Formation and Microfluidic Interfacing of Gels. Gels were formed by introducing a solution of type I collagen (from rat tail, 2.5–7 mg/ml; BD Biosciences), fibrinogen (15 and 30 mg/ml; Aniara), or Matrigel (10 mg/ml; BD Biosciences) into

[1]Corresponding author.
Manuscript received April 7, 2015; final manuscript received July 6, 2015; published online July 22, 2015. Assoc. Editor: Jeffrey Ruberti.

polydimethylsiloxane (PDMS; Sylgard 184 from Dow Corning) microfluidic channels on a glass slide (Fig. 1(*a*)). The PDMS microchannels were ~1 mm high, ~1 mm wide, and 1–3.4 cm long. The PDMS layer that formed the top wall of a channel had a thickness of 0.8–1.6 mm. We varied the elastic modulus of the PDMS by choosing the mass ratio of crosslinking agent to base polymer to be 1:5, 1:10, or 1:20. PDMS was cured at 60 °C for at least 1 day to ensure its mechanical properties reached limiting values. All microchannels had 6-mm-diameter wells cut into both ends.

We allowed the precursor solution in the PDMS channels to gel at room temperature (~23 °C) or in a CO_2 incubator (37 °C) for 30 min before adding phosphate-buffered saline (PBS) to the wells adjacent to the gel. The wells were then interfaced to separate reservoirs of PBS with PE-50 polyethylene tubing, and these reservoirs were placed on jacks that could be raised or lowered in tandem to change the hydrostatic pressure exerted at both ends of the gel.

Measurement of Interstitial Fluid Pressure. To measure interstitial fluid pressure within a gel, we applied our recently described noninvasive technique that relies on scanning white-light interferometry to detect the displacement of the walls of a microfluidic device under pressure [12,13]. Interferometric microscopy uses the interference between reference and reflecting light beams to map the absolute height of the upper surface of a sample, with a vertical resolution of ~5 nm [14]. Before imaging, we taped the glass slide (with its PDMS channel and gel) and its two lines of PE-50 tubing onto the stage of the interferometric microscope (NewView 6300; Zygo) to isolate the sample from any vibrations. With both PBS reservoirs held at 0 Pa (atmospheric pressure), we imaged the middle region of the PDMS outer surface at least three times in succession with a 2.5×/0.075 Nikon interferometric objective, until a stable baseline was reached. We then raised both reservoirs to the same pressure P_0 (245 or 490 Pa) and continued to image the same area. Finally, we repeated the imaging sequence, but with the reservoir pressures starting at the positive value and then suddenly lowered back to 0 Pa. For most gels, images were recorded every ~4 s, and at least 20 images were taken for each sequence (i.e., 20 images for a pressure increase, followed by 20 images for a pressure decrease). All imaging took place at room temperature.

We have previously shown that the displacement at a given pixel in an image is proportional to the interstitial pressure at that point [12]. Thus, the displacement and interstitial pressure have the same dependence with time (up to a multiplicative constant).

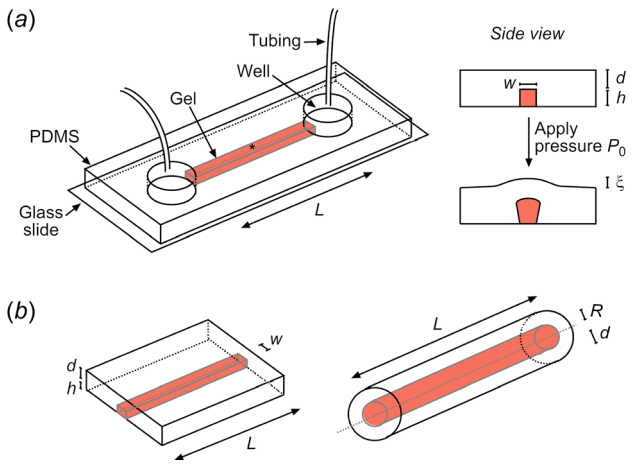

Fig. 1 (*a*) Experimental setup. Gels were formed in PDMS channels (top wall thickness *d*) with linear dimensions *L* × *w* × *h* that lay on top of a rigid glass slide. A pressure step P_0 was applied to both ends of the gel via tubing, and the distension $\xi(t)$ of the upper PDMS wall structure was measured at the center location denoted by an asterisk. (*b*) Computational geometries. Models of rectangular channels consisted of the experimental setup without tubing or wells; gel displacements were set to zero along the bottom plane. Models of cylindrical channels (radius *R*) were allowed to deform equally in all radial directions; gel displacements were not constrained to be zero along the cylindrical axis.

Measurement of Gel Hydraulic Permeability. We measured the flow rate of saline across collagen gels at room temperature under a pressure difference of ~4 cm H_2O. Application of Darcy's Law

$$\mathbf{v} = -k_{\text{gel}} \nabla P \tag{1}$$

yielded the hydraulic permeability k_{gel} for each gel. Here, $\mathbf{v}$ is the average interstitial flow velocity, and P is the interstitial fluid pressure. For fibrin and Matrigel, the permeabilities were too small to be measured precisely.

Numerical Modeling. Using COMSOL MULTIPHYSICS ver. 3.5 a (COMSOL), we constructed finite-element models of the experimental setup, with a porous medium (the gel) bonded to a rigid surface (the glass coverslip) on one side and to a deformable channel (the PDMS device) on three sides (Fig. 1(*b*)). The governing equations for the gel consisted of

$$\frac{\partial \varepsilon_{ii}}{\partial t} = k_{\text{gel}} \nabla^2 P \tag{2}$$

$$\frac{\partial \sigma_{ij}}{\partial x_i} = 0 \tag{3}$$

$$\sigma_{ij} = \frac{2G_{\text{gel}}\nu}{1-2\nu}\varepsilon_{kk}\delta_{ij} + 2G_{\text{gel}}\varepsilon_{ij} - P\delta_{ij} \tag{4}$$

where $\boldsymbol{\sigma}$ and $\boldsymbol{\varepsilon}$ are the stress and strain tensors, and G_{gel} and ν are the shear modulus and Poisson's ratio of the gel. Equations (2)–(4) are the fundamental laws of linear poroelasticity with incompressible constituents [7] and were implemented in COMSOL using the exact analogy with linear thermoelasticity [15]. In our notation, the stress tensor $\boldsymbol{\sigma}$ includes contributions from pore pressure and from the elastic stress that results from deformation of the gel.

The governing equations for the PDMS that surrounds a gel were

$$\sigma'_{ij} - \frac{1}{3}\sigma'_{kk}\delta_{ij} = \frac{2E_{\text{PDMS}}}{3}\varepsilon'_{ij} \tag{5}$$

where $\boldsymbol{\sigma}'$ and $\boldsymbol{\varepsilon}'$ are the stress and strain tensors, and E_{PDMS} is the Young's modulus. Equation (5) assumes that PDMS is incompressible, and required the use of models that treated the trace of the stress tensor as an independent parameter. The stress fields in the gel and PDMS were coupled by assuming that the gel stress acted as a load at the PDMS–gel interface

$$\sigma_{ij} = \sigma'_{ij} \tag{6}$$

At the glass–gel interface, displacements were constrained to be zero.

For each model, we solved Eqs. (2)–(6) for the time-dependent interstitial fluid pressure, gel deformation, and PDMS deformation when a sudden pressure of up to 735 Pa was applied at the ends of the gel; the initial pressure in the gel and PDMS was 0 Pa. To understand the effect of the rigid boundary condition at the glass–gel interface on interstitial pressure dynamics, we also modeled the deformation of a gel within a cylindrical PDMS channel, in which the gel was bonded only to deformable surfaces (Fig. 1(*b*)). From each solution, we obtained the time-dependent

distension $\xi(t)$ at the midpoint of the outer PDMS surface; this location corresponded to the one imaged experimentally with interferometric microscopy. We fit each $\xi(t)$ to a decaying exponential to obtain an equilibrium distension ξ_∞ and a time constant τ; in some cases, we had to neglect the initial 10–20% of the distension–time curve to obtain a reliable fit. To confirm mesh independence, we refined the meshes until a two-fold increase in the degrees-of-freedom led to $\leq 3\%$ and $\leq 0.1\%$ change in ξ_0 (the distension immediately after pressure was applied), ξ_∞, and τ for rectangular and cylindrical channels, respectively.

Results

Characteristics of Experimental Distension–Time Plots. When we imposed a sudden pressure increase at the ends of a gel (type I collagen, fibrin, Matrigel) in a microfluidic PDMS channel, the outer surface of the PDMS immediately distended very slightly outward, as shown by interferometric microscopy (Figs. 2(*a*) and 2(*b*)). The distension then increased over time until an asymptotic value was reached. Given that the distension is proportional to the local interstitial fluid pressure; our data implied that the pressure also displayed the same dependence on time, i.e., an initial jump followed by a slow, limited rise.

For nearly all samples (see Fig. 2(*a*) for a representative case), the measured time-lapse distensions $\xi(t)$ fit the following form very well:

$$\xi(t) = \xi_\infty - \text{const.} \cdot e^{-t/\tau} \tag{7}$$

In a few samples (see Fig. 2(*b*) for the most obvious case), the initial time-dependence of distension was more sigmoidal than linear, and only the data at later times fit Eq. (7) well. The goodness of fit was routinely ≥ 0.9. For collagen gels with concentrations of 2.5–7 mg/ml, the time constants τ ranged from 4 to 25 s (Table 1). For fibrin gels with concentrations of 15 and 30 mg/ml and for Matrigel, the values of τ were typically much larger, on the order of 100 s or more. Smaller gel hydraulic permeabilities and larger gel lengths tended to yield larger τ; the magnitude of the imposed pressure had no effect on τ. Sigmoidal distension–time curves were only observed for gels in which the initial distension ξ_0 was much smaller than the fitted asymptotic value ξ_∞.

These characteristics of the interstitial pressure dynamics—the existence of a delayed, sigmoidal pressure rise in some gels, the slower rise in longer gels, and the indifference to magnitude of imposed pressure—suggested that a diffusive transport process (i.e., "diffusion" of interstitial pressure) may underlie the observed findings. We surmised that the imposed external pressure needed to diffuse into the gel before the central region of the PDMS channel could distend outwards. Nevertheless, diffusion of interstitial pressure could not account for the instantaneous distension ξ_0, which should always be zero in a diffusive process.

Computational Modeling of Poroelastic Dynamics. To better understand the origin of the interstitial pressure rise and the factors that influence it, we solved finite-element models that corresponded to the experimental setup (Supplemental Table S1, available under the "Supplemental Data" tab for this paper on the ASME Digital Collection). When constructing a model, we chose a range of values that encompassed those expected for the experimental setup (e.g., for the hydraulic permeability of the gel and the elastic modulus of PDMS). Since the Poisson's ratio ν is generally not reported in the literature for soft extracellular matrix gels, we used a broad range from 0 to 0.499.

The general features of the distension–time curves for these computational models matched those from experimental data (Figs. 2(*c*) and 2(*d*)). Most distension–time curves fit the exponential form of Eq. (7) very well, with goodness of fit ≥ 0.99. Models with longer or less permeable gels had larger time constants for the pressure rise, and the time constants did not depend on the magnitude of imposed pressure. In some models, the initial

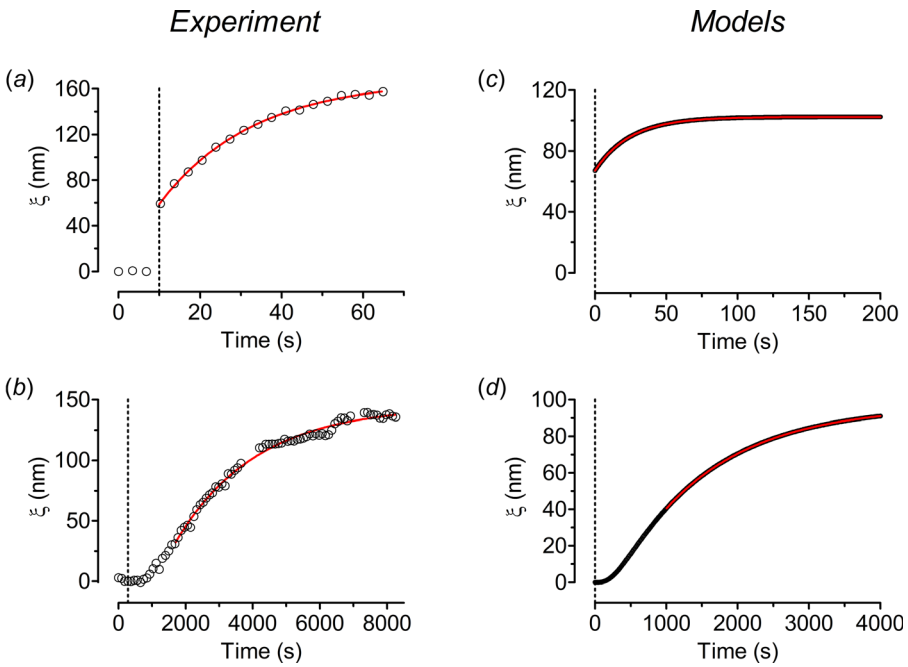

Fig. 2 Representative distension–time plots from experiments and computational models. Data were obtained from the boldfaced experimental and modeling cases in Table 1 and Supplemental Table S1, available under the "Supplemental Data" tab for this paper on the ASME Digital Collection; the modeling cases were chosen to give qualitatively similar time-dependences to those observed experimentally. (*a*) and (*b*) Experimental data. (*c*) and (*d*) Computational results. Dotted lines denote the times at which external pressure was applied; solid (red) curves indicate best fits to Eq. (7).

Table 1 Parameters for experimentally analyzed gels and devices. The linear dimensions (*L*, *w*, *h*, *d*) are defined in Fig. 1(*a*). For all but the last fibrin gel, the distensions and time constants are the averages of values from a step increase or decrease in external pressure; for that fibrin gel, only the values from a step pressure increase are listed. Italicized values were estimated by fitting experimental data to master curves (see Results). Boldfaced cases were plotted in Fig. 2. Col: collagen; Fbn: fibrin; Mg: Matrigel; and n.d.: not done.

Gel	L (mm)	w (mm)	h (mm)	d (mm)	P_0 (Pa)	k_{gel} (cm^4/dyn s)	G_{gel} (Pa)	E_{PDMS} (MPa)	ξ_0 (nm)	ξ_∞ (nm)	τ (s)
Col	**33.5**	**0.98**	**1.13**	**1.02**	**245**	**1.37×10^{-8} (*1.36×10^{-8}*)**	***313***	***1.94***	**57.3**	**166.9**	**23.4**
Col	33.5	0.98	1.18	1.17	245	1.86×10^{-8} (*1.61×10^{-8}*)	*900*	*2.16*	21.1	142.8	13.0
Col	33	0.98	1.18	1.43	490	6.54×10^{-8} (*5.16×10^{-8}*)	*89.0*	*3.14*	129.6	160.8	12.9
Col	33	0.98	1.09	1.34	245	2.23×10^{-8} (*2.09×10^{-8}*)	*680*	*0.69*	10.7	335.2	25.4
Col	33.5	0.98	1.20	1.51	490	1.22×10^{-7} (*1.03×10^{-7}*)	*31.8*	*3.22*	142.8	153.5	16.9
Col	33	0.97	1.24	1.54	490	3.76×10^{-8} (*3.91×10^{-8}*)	*135*	*3.62*	111.5	143.2	12.8
Col	34	0.98	1.25	1.47	245	2.37×10^{-8} (*2.27×10^{-8}*)	*228*	*2.44*	63.2	113.1	17.1
Col	34	0.98	1.23	1.33	245	8.32×10^{-8} (*6.37×10^{-8}*)	*522*	*2.33*	38.7	125.7	3.9
Fbn	34	0.96	1.21	1.19	490	*2.55×10^{-10}*	*2295*	*2.38*	10.7	268.2	655.1
Fbn	10	0.97	1.12	0.84	490	*6.39×10^{-10}*	*1750*	*1.83*	231.9	423.4	65.7
Fbn	10	0.98	1.10	1.30	490	*6.20×10^{-11}*	*13600*	*3.33*	27.7	145.1	195.2
Fbn	10	0.98	1.09	1.19	490	*7.13×10^{-11}*	*10800*	*3.07*	36.2	168.7	190.8
Fbn	**34**	**0.97**	**1.10**	**0.89**	**245**	**n.d.**	**n.d.**	***2.46***	**−1.6**	**143.4**	**2404**
Mg	34	0.97	1.21	0.81	490	*1.43×10^{-9}*	*96.6*	*2.46*	274.4	380.5	479.5

portion of the curves was sigmoidal, and here the initial distension ξ_0 was always much smaller than the asymptotic one ξ_∞.

To see whether these features were unique to a rectangular microfluidic geometry, we also analyzed models in which a cylindrical gel was completely surrounded by a coaxial tube of PDMS (Supplemental Table S2, available under the "Supplemental Data" tab for this paper on the ASME Digital Collection). Again, Eq. (7) was an outstanding fit to the distension–time curves, and the findings in rectangular channels with one rigid wall also held in cylindrical ones with no rigid wall.

Scaling Laws for the Poroelastic Time Constants. To understand the physical origin of the interstitial pressure dynamics, we first assumed that the top wall of the PDMS channels distended with underlying interstitial pressure but that—given the extremely small distensions (on the order of 100 nm)—the PDMS distension did not itself affect the pressure dynamics in the gel. In this case, two uncoupled equations determine the outcome [7,13]

$$\frac{\partial P}{\partial t} = k_{gel} B_{gel} \nabla^2 P - \frac{1}{3}\frac{\partial \sigma_{ii}}{\partial t} \tag{8}$$

$$\xi(t) \approx \frac{\xi_\infty}{P_0} P(t) \tag{9}$$

Here, $B_{gel} = (2/3)G_{gel}(1+\nu)/(1-2\nu)$ is the drained bulk modulus of the gel, and P_0 is the pressure imposed at the ends of the gel. In this case, the time constant for interstitial pressure rise should take the form $\tau \approx L^2/8k_{gel}B_{gel}$, where L is the length of the gel. Computational results (Fig. 3(*a*)) showed that while τ and $L^2/8k_{gel}B_{gel}$ are correlated, the former is smaller than the latter by nearly two orders of magnitude. Thus, the PDMS wall does not act solely as a boundary that distends passively under pressure from the gel, but its distension must influence the gel pressure as well.

One way in which the distension of the PDMS wall may affect interstitial pressure is by altering the movement of the small volume of extra fluid required for distension. The volumetric interstitial flow rate is given by Darcy's Law and is approximately $2k_{gel}AP_0/L$, where A is the cross-sectional area of the gel. This flow provides the fluid required for the volume increase ΔV of the gel as a result of PDMS distension. Thus, one expects the time constant to be given by $L\Delta V/2k_{gel}AP_0$, which equals $L^2\xi_\infty/2k_{gel}hP_0$ for rectangular channels, where h is the thickness of the gel; for cylindrical channels, the time constant should be $L^2\xi_\infty/k_{gel}RP_0$, where R is the radius of the gel. This scaling analysis provides a correct order-of-magnitude estimate, but still has substantial scatter (Fig. 3(*b*)).

The above analysis assumes that axial pressure diffusion (i.e., parallel to the PDMS channel) is the only determinant of the time constant. In principle, transverse pressure diffusion from the centerline of the gel to the PDMS–gel interface may also contribute to the interstitial pressure dynamics. Thus, we fit the calculated time constants to linear combinations of terms of the form $(\text{length})^2/k_{gel}\cdot(\text{elastic modulus})$, where the length is the length or height of the gel, and the modulus is that of the gel or PDMS. Remarkably, the data fit the following expressions almost perfectly (Fig. 3(*c*)):

$$\tau = \tau_\parallel + \tau_\perp \tag{10}$$

$$\tau_\parallel = 0.30\frac{L^2}{k_{gel}E_{PDMS}}\ (\text{rectangular channel}) \tag{11a}$$

$$\tau_\perp = 0.036\frac{h^2}{k_{gel}G_{gel}}\ (\text{rectangular channel}) \tag{11b}$$

$$\tau_\parallel = 0.40\frac{L^2}{k_{gel}E_{PDMS}}\ (\text{cylindrical channel}) \tag{12a}$$

$$\tau_\perp = 0.13\frac{R^2}{k_{gel}G_{gel}}\ (\text{cylindrical channel}) \tag{12b}$$

The decomposition of the time constant into axial ($\tau_\parallel$) and transverse ($\tau_\perp$) contributions implies that, when the gel is pressurized, the interstitial pressure must diffuse along and across the gel before the PDMS can distend. In some models, axial or transverse pressure diffusion is rate-limiting, while in others, both modes of diffusion are important (Fig. 3(*c*), inset). Notably, even though the final distension ξ_∞ is very small in all cases (~0.01% of the gel thickness), the effects of interstitial pressure diffusion may be

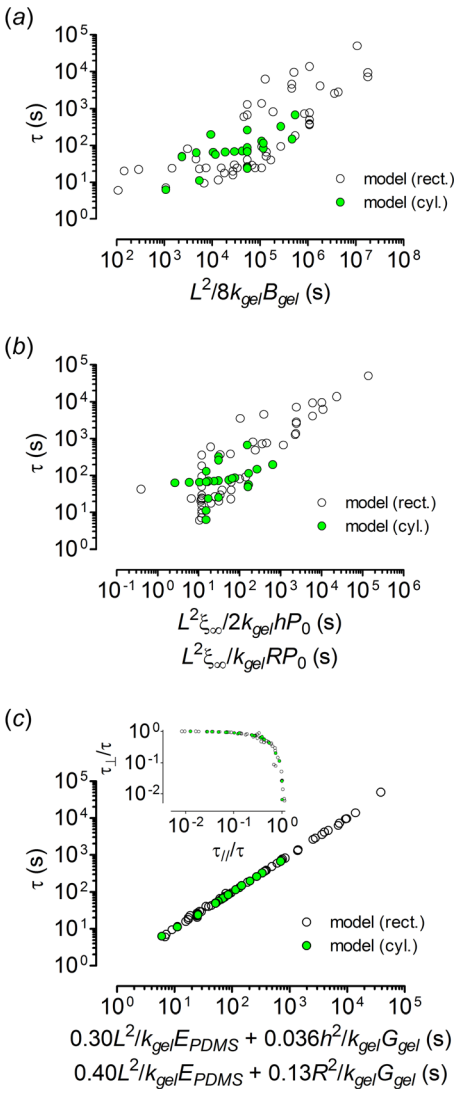

Fig. 3 Plots of time constant τ versus proposed scaling expressions. (*a*) Scaling law that incorporates gel poroelastic constants and assumes axial pressure diffusion is rate-limiting. (*b*) Scaling law that incorporates PDMS distension and assumes axial fluid transport is rate-limiting. (*c*) Scaling law that assumes axial and transverse pressure diffusion contribute to τ. Open circles: rectangular channels and solid (green) circles: cylindrical channels.

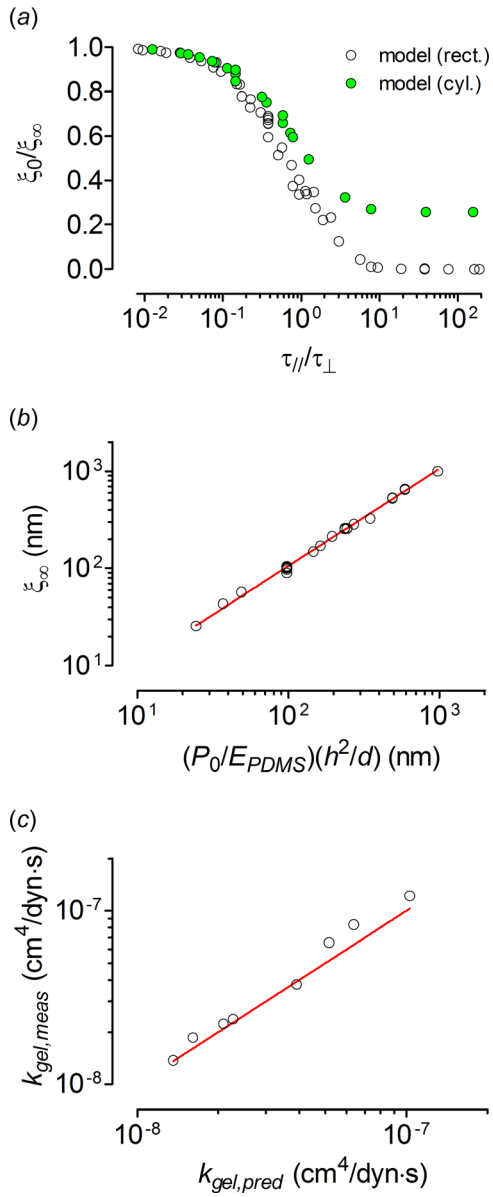

Fig. 4 Scaling behavior of the initial and equilibrium PDMS distensions ξ_0 and ξ_∞, respectively, and application to the prediction of a gel's hydraulic permeability k_{gel}. (*a*) ξ_0/ξ_∞ versus $\tau_{//}/\tau_\perp$. (*b*) Scaling law for ξ_∞ that assumes linear response to interstitial fluid pressure, for rectangular channels. The solid (red) line plots the empirical fit of Eq. (14). (*c*) Plot of measured k_{gel} for collagen gels versus the values predicted from the computed scaling laws. The solid (red) line plots equality.

considerable, and the attainment of maximum interstitial fluid pressure may be severely retarded.

Origin of the Initial Jump in Interstitial Fluid Pressure. Although the idea of interstitial pressure diffusion appears to explain much of the pressure dynamics, it fails to explain how interstitial fluid pressure at the central region of the gel can increase instantaneously when the external pressure is applied at the ends (Fig. 2(*a*)). This initial increase is the result of undrained deformation of the gel, in which no interstitial fluid has flowed yet, and the gel acts transiently as a solid with Poisson's ratio of 0.5 [7]. The softer the gel, the greater the initial distension, because the interstitial fluid pressure must bear a greater portion of the applied load to maintain mechanical equilibrium. Surprisingly, a plot of the ratio of initial to final PDMS distensions ξ_0/ξ_∞ versus the ratio of time constants $\tau_{||}/\tau_\perp$ for all computational models appeared to collapse onto a master curve (Fig. 4(*a*)). Models in which axial pressure diffusion is fast (i.e., $\tau_{||}/\tau_\perp \ll 1$) had large initial distensions (i.e., $\xi_0/\xi_\infty \approx 1$). Although this result may appear intuitive, the initial change is not a diffusive one, and a convincing explanation of the link between elastic deformations and poroelastic transport times remains elusive.

Determination of Gel Poroelastic Constants. The outstanding fit of Eqs. (10) and (11) to the computational results suggests that one may be able to obtain the poroelastic constants of a gel in a microfluidic PDMS channel from experimental measurements of PDMS distension over time. Our experimental and computational results imply that the distension–time curves can be largely described by three values: the initial distension ξ_0, the asymptotic distension ξ_∞, and the time constant τ. The desired poroelastic constants are the permeability k_{gel} and modulus G_{gel}.

From the distension ξ_∞, one can determine the PDMS modulus E_{PDMS}. Because extracellular matrix gels are much softer than

PDMS is, and because the interstitial fluid pressure approaches the external pressure P_0 at long times, ξ_∞ must have the form

$$\xi_\infty = \frac{P_0}{E_{\text{PDMS}}} f(h, L, \ldots) \tag{13}$$

where f is a function solely of the PDMS geometry. For the rectangular channels used in experiments

$$\xi_\infty = 1.06 \frac{P_0}{E_{\text{PDMS}}} \frac{h^2}{d} \tag{14}$$

is an outstanding fit to the computational data, where d is the thickness of the PDMS wall (Fig. 4(*b*)).

Thus, the procedure for deducing the gel poroelastic constants from distension–time data in rectangular PDMS microfluidic channels is as follows. First, using the fitted asymptotic distension ξ_∞ and Eq. (14), we obtain E_{PDMS}. Second, using the ratio ξ_0/ξ_∞ and the master curve in Fig. 4(*a*), we obtain $\tau_{\|}/\tau_{\perp}$; in conjunction with Eq. (11) and E_{PDMS}, this ratio yields G_{gel}. Finally, from the measured time constant τ, we can obtain $\tau_{\|}$ and $\tau_{\perp}$, and thus obtain k_{gel} from Eq. (11).

We applied this procedure to the gels described in Table 1, and the predicted values for k_{gel} and G_{gel} (and E_{PDMS}) are listed in italics. For the collagen gels, we also directly measured the hydraulic permeabilities, and the predicted values slightly underestimated the measured ones by an average of 11% (Fig. 4(*c*)). For the fibrin gels, the deduced k_{gel} agree well with our previously reported values [16]. The reported values of permeability for Matrigel span orders of magnitude [17,18], probably because Matrigel is so soft that some permeability assays unintentionally deform the gel and thereby lower k_{gel}; our deduced value lies within the reported range.

The predicted gel moduli G_{gel} also matched closely with previously reported values and scaling laws. For instance, collagen gels that were formed at 37 °C had substantially lower moduli than those formed at room temperature [19,20]. Matrigel was extremely soft (~100 Pa), while fibrin gels were much stiffer (2 kPa and 12 kPa for 15 mg/ml and 30 mg/ml gels, respectively). Linear fits of log-transformed moduli and gel concentrations c yielded $G_{\text{gel}} \sim c^{2.2}$ for collagen and $G_{\text{gel}} \sim c^{2.6}$ for fibrin, which is in good agreement with published scaling laws [20,21].

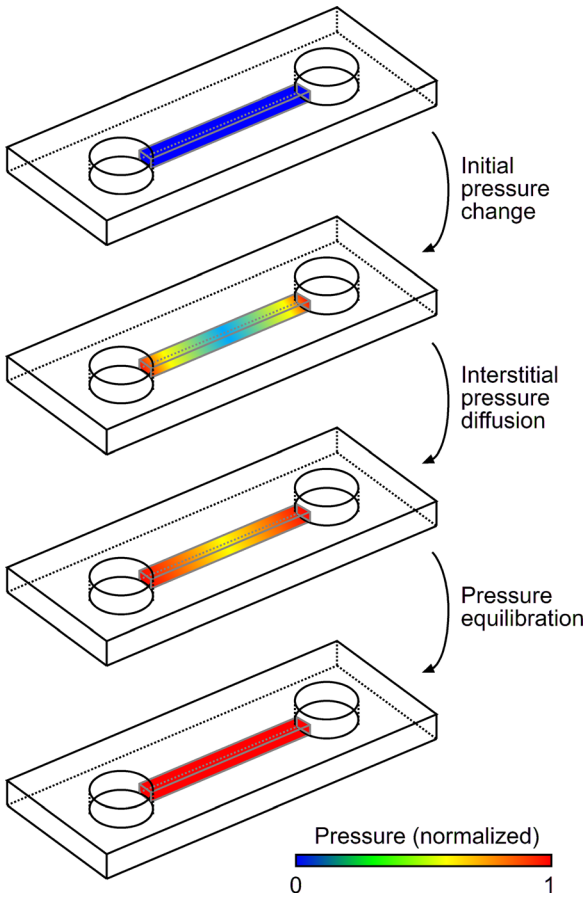

Fig. 5 Stages in the reaction of an encapsulated gel to externally applied pressure. A gel that is initially at zero pressure deforms instantaneously, thereby establishing an initial interstitial pressure distribution. Axial and transverse pressure diffusion then take place, until the pressure reaches its steady-state distribution. The color maps show the ratio of interstitial to applied pressures, at various times.

Discussion

Response of Interstitial Pressure to a Change in External Fluid Pressure. Our results show that, for gels that are in contact with a deformable surface, interstitial fluid pressure does not respond instantaneously and completely to a change in external fluid pressure. Instead, the pressure dynamics follow a series of interlinked steps (Fig. 5). First, an instantaneous pressure jump will take place, as the gel acts initially as an incompressible solid. Next, interstitial pressure diffuses through the gel in two modes: one that is governed only by the poroelastic constants of the gel, and one that couples the hydraulic permeability of the gel with the elastic modulus of the boundary material. The gels analyzed here had large aspect ratios, and the two modes of interstitial pressure change could be identified with transverse and axial pressure diffusion, respectively. For gels that have less elongated geometries, we expect the elastic properties of the boundary to remain important in interstitial pressure changes, although the decomposition of pressure diffusion into distinct modes may be less clear. Finally, at long times, the interstitial pressure will reach a steady distribution.

Dependence of Interstitial Pressure Time Constants on Gel and Boundary Properties. Previous studies have examined how the presence of a permeable, but rigid, boundary affects interstitial pressure dynamics in vascularized tumors [22,23]. In these studies, two time constants for interstitial pressure changes were apparent: an "intrinsic" one that depends solely on the properties of the interstitium, and one that combines the properties of the interstitium and boundary.

Our current study examines the complementary situation, in which an impermeable, but deformable, boundary surrounds the porous material. In line with past work on equilibration times in poroelastic tissues [8,24], we have found that the overall time constant for interstitial pressure changes can be decomposed into two terms, both of which have the form $(\text{length})^2/k_{\text{gel}}\cdot(\text{elastic modulus})$. Again, one time constant ($\tau_{\perp}$) depended on the gel's properties, while the other ($\tau_{\|}$) depended on both gel and boundary.

Despite this similarity, our findings differ from those of previous studies in several ways. First, both time constants were much smaller than the intrinsic one $L^2/8k_{\text{gel}}B_{\text{gel}}$ expected from the gel's poroelastic constants. This result suggests that the deformable PDMS boundary enhances the diffusion of interstitial pressure and strain. Second, the two time constants could be identified with pressure equilibration along distinct directions. The PDMS wall only affects pressure diffusion along the axial direction (i.e., parallel to the boundary), while the mechanical properties of the gel only affect diffusion in the transverse direction. Third, the time constant for axial pressure diffusion depends on the elastic modulus E_{PDMS}, rather than the compliance ξ_∞/P_0, of the PDMS wall. Altogether, these results indicate that distension of the PDMS wall accelerates axial pressure diffusion by stretching the underlying gel. Because PDMS is much stiffer than the gels we studied, it

enhances the mechanical interaction between different regions of a gel.

Relevance to Microscale Cell Cultures and Tissues. These findings suggest that one may need to consider interstitial pressure dynamics when coupling cell-laden microscale gels in microfluidic devices to external pressures. For example, a 5-mm-long fibrin gel with embedded endothelial cells (a format that can be used to study how interstitial flow affects vasculogenesis [2,25]) could have time constants on the order of minutes for changes in interstitial pressure. While such dynamics would be expected to decay away if the imposed pressure is held constant, interstitial pressure diffusion would become important if the imposed pressure is pulsatile with a period of minutes or shorter. We note that interstitial pressure dynamics can be significant, even though the strain ξ_∞/h of the gel is extremely small ($\sim$0.01%) and typically ignored. Moreover, these dynamics become more pronounced in gels that are less stiff (e.g., in very dilute gels), since $\tau_\perp$ is inversely proportional to G_{gel}.

The time constant for interstitial pressure changes is inversely proportional to the hydraulic permeability of the gel. For synthetic polymer gels (e.g., polyethylene glycol-based gels), the permeabilities can be even lower than the ones we analyzed here [26], and the interstitial pressure changes will be correspondingly slower. When one considers that cells can actively exert stress against their surroundings, it seems likely that the interstitial pressure at any given location and time will be the integrated result of delayed pressure changes that propagate from many locations. Deformable boundaries in biological systems include blood and lymphatic vessels, epithelial ducts, epidermis, cell membranes, and air bubbles [27]. In principle, each of these boundaries can locally affect the diffusion of interstitial pressure (e.g., during the infusion of drug solutions into a tissue [28]). Time-resolved interstitial fluid pressure maps may be needed to better understand how pressure changes affect cell behavior in these and similar situations.

Application to Optical Elastography. By elucidating the scaling relations for the poroelastic dynamics, this study provides a way to infer the properties of gels in a noninvasive manner from distension–time measurements. For highly resistive gels, direct measurement of hydraulic permeability requires the use of large pressures across thin films to increase the flow rates across the gel to a detectable level. These flow conditions can lead to compaction of the gel, nonuniformity in the pressure gradient, and/or solute polarization [17]. While the estimation of permeability from stress relaxation times is certainly not new, previous methods often involve large nonuniform strain fields, such as during indentation or bending of gels, and corrections for deformation-induced changes in permeability often must be included [29–31]. Our method provides pressure relaxation times under infinitesimal strains, and thus provides the permeability of a gel under its native state. The close agreement between experimental and predicted values of k_{gel} gives us confidence about the soundness of our analyses.

For extremely impermeable gels (such as the one in Fig. 2(*b*)), for which measurement of pressure time constants may be impractical, it may be possible to realize the same idea using an oscillatory waveform instead of the pulsed approach described here. In this case, one would vary the external pressure at the ends of the gel and detect the oscillatory motion of the outer PDMS wall. By sweeping the frequency and extracting phase and amplitude information, one can determine the complex response function of the system [32,33]. The oscillatory approach could provide better signal-to-noise ratio because it is insensitive to drift, and it may also shorten the total measurement time.

Acknowledgment

We thank Celeste Nelson and Victor Varner for experimental assistance. This work was supported by a Dean's Catalyst Award from the College of Engineering at Boston University.

Nomenclature

A = cross-sectional area of PDMS channel and gel
B_{gel} = bulk modulus of gel
c = concentration of gel
d = thickness of PDMS wall above gel
E_{PDMS} = Young's modulus of PDMS
G_{gel} = shear modulus of gel
h = height of PDMS channel and gel
k_{gel} = hydraulic permeability of gel
L = length of PDMS channel and gel
P = interstitial fluid pressure
P_0 = imposed pressure at ends of gel
R = radius of PDMS channel and gel (only for cylindrical models)
t = time
$\mathbf{v}$ = interstitial flow velocity
w = width of PDMS channel and gel
ΔV = equilibrium volume change of gel after application of pressure
$\boldsymbol{\varepsilon}$, ε_{ij} = infinitesimal strain tensor of gel
$\boldsymbol{\varepsilon}'$, ε'_{ij} = infinitesimal strain tensor of PDMS
ν = Poisson's ratio of gel
ξ = distension of outer PDMS wall
ξ_0, ξ_∞ = initial and equilibrium (fitted) distensions of outer PDMS wall after application of pressure
$\boldsymbol{\sigma}$, σ_{ij} = Cauchy stress tensor of gel
$\boldsymbol{\sigma}'$, σ'_{ij} = Cauchy stress tensor of PDMS
τ, $\tau_\parallel$, $\tau_\perp$ = overall, axial, and transverse time constants for changes in interstitial fluid pressure

References

[1] Swartz, M. A., and Fleury, M. E., 2007, "Interstitial Flow and Its Effects in Soft Tissues," Annu. Rev. Biomed. Eng., **9**, pp. 229–256.
[2] Helm, C.-L. E., Fleury, M. E., Zisch, A. H., Boschetti, F., and Swartz, M. A., 2005, "Synergy Between Interstitial Flow and VEGF Directs Capillary Morphogenesis In Vitro Through a Gradient Amplification Mechanism," Proc. Natl. Acad. Sci. U. S. A., **102**(44), pp. 15779–15784.
[3] Tien, J., Truslow, J. G., and Nelson, C. M., 2012, "Modulation of Invasive Phenotype by Interstitial Pressure-Driven Convection in Aggregates of Human Breast Cancer Cells," PLoS One, **7**(9), p. e45191.
[4] Detournay, E., and Cheng, A. H.-D., 1993, "Fundamentals of Poroelasticity," *Comprehensive Rock Engineering: Principles, Practice and Projects* (Analysis and Design Method, Vol. II), C. Fairhurst, ed., Pergamon, New York, pp. 113–171.
[5] Quinn, T. M., 2013, "Flow-Induced Deformation of Poroelastic Tissues and Gels: A New Perspective on Equilibrium Pressure-Flow-Thickness Relations," ASME J. Biomech. Eng., **135**(1), p. 011009.
[6] Bowen, R. M., 1980, "Incompressible Porous Media Models by Use of the Theory of Mixtures," Int. J. Eng. Sci., **18**(9), pp. 1129–1148.
[7] Wang, H. F., 2000, *Theory of Linear Poroelasticity With Applications to Geomechanics and Hydrogeology*, Princeton University, Princeton, NJ.
[8] Mow, V. C., Kuei, S. C., Lai, W. M., and Armstrong, C. G., 1980, "Biphasic Creep and Stress Relaxation of Articular Cartilage in Compression: Theory and Experiments," ASME J. Biomech. Eng., **102**(1), pp. 73–84.
[9] Mow, V. C., Holmes, M. H., and Lai, W. M., 1984, "Fluid Transport and Mechanical Properties of Articular Cartilage: A Review," J. Biomech., **17**(5), pp. 377–394.
[10] Hsu, Y.-H., Moya, M. L., Hughes, C. C. W., George, S. C., and Lee, A. P., 2013, "A Microfluidic Platform for Generating Large-Scale Nearly Identical Human Microphysiological Vascularized Tissue Arrays," Lab Chip, **13**(15), pp. 2990–2998.
[11] Polacheck, W. J., Charest, J. L., and Kamm, R. D., 2011, "Interstitial Flow Influences Direction of Tumor Cell Migration Through Competing Mechanisms," Proc. Natl. Acad. Sci. U. S. A., **108**(27), pp. 11115–11120.
[12] Ozsun, O., Thompson, R. L., Ekinci, K. L., and Tien, J., 2014, "Non-Invasive Mapping of Interstitial Fluid Pressure in Microscale Tissues," Integr. Biol., **6**(10), pp. 979–987.
[13] Ozsun, O., Yakhot, V., and Ekinci, K. L., 2013, "Non-Invasive Measurement of the Pressure Distribution in a Deformable Micro-Channel," J. Fluid Mech., **734**, p. R1.
[14] Deck, L., and de Groot, P., 1994, "High-Speed Noncontact Profiler Based on Scanning White-Light Interferometry," Appl. Opt., **33**(31), pp. 7334–7338.
[15] Norris, A., 1992, "On the Correspondence Between Poroelasticity and Thermoelasticity," J. Appl. Phys., **71**(3), pp. 1138–1141.
[16] Wong, K. H. K., Truslow, J. G., Khankhel, A. H., Chan, K. L. S., and Tien, J., 2013, "Artificial Lymphatic Drainage Systems for Vascularized Microfluidic Scaffolds," J. Biomed. Mater. Res. A, **101**(8), pp. 2181–2190.
[17] McCarty, W. J., and Johnson, M., 2007, "The Hydraulic Conductivity of Matrigel," Biorheology, **44**(5–6), pp. 303–317.

[18] Ng, C. P., and Pun, S. H., 2008, "A Perfusable 3D Cell-Matrix Tissue Culture Chamber for In Situ Evaluation of Nanoparticle Vehicle Penetration and Transport," Biotechnol. Bioeng., **99**(6), pp. 1490–1501.
[19] Chrobak, K. M., Potter, D. R., and Tien, J., 2006, "Formation of Perfused, Functional Microvascular Tubes In Vitro," Microvasc. Res., **71**(3), pp. 185–196.
[20] Yang, Y.-L., Leone, L. M., and Kaufman, L. J., 2009, "Elastic Moduli of Collagen Gels Can be Predicted From Two-Dimensional Confocal Microscopy," Biophys. J., **97**(7), pp. 2051–2060.
[21] Carr, M. E., Shen, L. L., and Hermans, J., 1976, "A Physical Standard of Fibrinogen: Measurement of the Elastic Modulus of Dilute Fibrin Gels With a New Elastometer," Anal. Biochem., **72**(1–2), pp. 202–211.
[22] Leiderman, R., Barbone, P. E., Oberai, A. A., and Bamber, J. C., 2006, "Coupling Between Elastic Strain and Interstitial Fluid Flow: Ramifications for Poroelastic Imaging," Phys. Med. Biol., **51**(24), pp. 6291–6313.
[23] Netti, P. A., Baxter, L. T., Boucher, Y., Skalak, R., and Jain, R. K., 1995, "Time-Dependent Behavior of Interstitial Fluid Pressure in Solid Tumors: Implications for Drug Delivery," Cancer Res., **55**(22), pp. 5451–5458.
[24] Armstrong, C. G., Lai, W. M., and Mow, V. C., 1984, "An Analysis of the Unconfined Compression of Articular Cartilage," ASME J. Biomech. Eng., **106**(2), pp. 165–173.
[25] Kim, S., Lee, H., Chung, M., and Jeon, N. L., 2013, "Engineering of Functional, Perfusable 3D Microvascular Networks on a Chip," Lab Chip, **13**(8), pp. 1489–1500.
[26] Nguyen, Q. T., Hwang, Y., Chen, A. C., Varghese, S., and Sah, R. L., 2012, "Cartilage-Like Mechanical Properties of Poly (Ethylene Glycol)-Diacrylate Hydrogels," Biomaterials, **33**(28), pp. 6682–6690.
[27] Fung, Y. C., 1993, *Biomechanics: Mechanical Properties of Living Tissues*, Springer-Verlag, New York.
[28] Basser, P. J., 1992, "Interstitial Pressure, Volume, and Flow During Infusion Into Brain Tissue," Microvasc. Res., **44**(2), pp. 143–165.
[29] Chandran, P. L., and Barocas, V. H., 2004, "Microstructural Mechanics of Collagen Gels in Confined Compression: Poroelasticity, Viscoelasticity, and Collapse," ASME J. Biomech. Eng., **126**(2), pp. 152–166.
[30] Chiarelli, P., Basser, P. J., Derossi, D., and Goldstein, S., 1992, "The Dynamics of a Hydrogel Strip," Biorheology, **29**(4), pp. 383–398.
[31] Ateshian, G. A., and Weiss, J. A., 2010, "Anisotropic Hydraulic Permeability Under Finite Deformation," ASME J. Biomech. Eng., **132**(11), p. 111004.
[32] Charlaix, E., Kushnick, A. P., and Stokes, J. P., 1988, "Experimental Study of Dynamic Permeability in Porous Media," Phys. Rev. Lett., **61**(14), pp. 1595–1598.
[33] Sheng, P., and Zhou, M.-Y., 1988, "Dynamic Permeability in Porous Media," Phys. Rev. Lett., **61**(14), pp. 1591–1594.